Menthylamine synthesis via gold-catalyzed hydrogenation of menthone oxime

Demidova, Yu S.; Mozhaitsev, E. S.; Suslov, E. V.; Nefedov, A. A.; Saraev, A. A.; Volcho, K. P.; Salakhutdinov, N. F.; Simakov, A.; Simakova, I. L.; Murzin, D. Yu

Published in:
Applied Catalysis A: General

DOI:
10.1016/j.apcata.2020.117799

Published: 05/09/2020

Document Version
Accepted author manuscript

Document License
CC BY-NC-ND

Menthylamine synthesis via gold-catalyzed hydrogenation of menthone oxime

Yu.S. Demidova[1,2], E.S. Mozhaitsev[3], E.V. Suslov[3], A.A. Nefedov[2,3], A.A. Saraev[1,2], K.P. Volcho[2,3], N.F. Salakhutdinov[2,3], A. Simakov[4], I.L. Simakova[1*], D.Yu. Murzin[5]

[1]*Boreskov Institute of Catalysis, pr. Lavrentieva 5, 630090, Novosibirsk, Russia*

[2]*Novosibirsk State University, Pirogova 2, 630090, Novosibirsk, Russia*

[3]*Novosibirsk Institute of Organic Chemistry, pr. Lavrentieva 9, 630090, Novosibirsk, Russia*

[4]*Universidad Nacional Autónoma de México, Centro de Nanociencias y Nanotecnología, km. 107 carretera Tijuana a Ensenada, C.P. 22860, Ensenada, Baja California, México*

[5]*Process Chemistry Centre, Åbo Akademi University, FI-20500, Turku/Åbo, Finland*

[*]E-mail: simakova@catalysis.ru

ABSTRACT

In the current work gold nanoparticles supported on oxides (MgO, Al_2O_3, ZrO_2, TiO_2) were used for menthylamine synthesis via menthone oxime hydrogenation. An increase of the gold nanoparticles size and application of metal oxides with a strong basic character such as magnesia favored deoximation to menthone. Au/Al_2O_3 catalyst with the gold nanoparticles size of 2.0 nm afforded high catalytic activity and selectivity to menthylamine. The reaction kinetics including stereoselectivity to the reaction products and recyclability of the catalyst was studied using Au/Al_2O_3 in the temperature range 90-110ºC under hydrogen pressure of 5.5-7.5 bar. The catalytic behavior was influenced by the solvent nature, with higher selectivity to desired amine achieved using methanol. The reaction rate was pressure independent, while has first order with respect to menthone

oxime concentration. Stereoselectivity to menthylamines and menthones was independent on the reaction temperature and the hydrogen pressure.

*Keywords***:** oxime hydrogenation, terpenoids, menthylamine, gold catalyst, biomass, kinetics.

1. Introduction

Stereo-, regio- and chemoselective hydrogenation is of interest for synthesis of the desired products with a high efficiency. Widespread terpenoids form the largest group of natural compounds and are extensively applied as platform molecules in food, pharmaceutical and perfumery industries [1]. Terpenoids often contain asymmetric centers and several functional groups, including reducible ones. Development of selective catalysts for reduction of different functional groups in terpenoids aiming at production of valuable intermediates for fine chemicals and pharmaceuticals is a challenging task. Hydrogenation of monoterpene oximes is one of the key steps in the synthesis of valuable compounds. There is a variety of products that can be obtained starting from oximes including carbonyl compounds and amines. For instance, deoximation of carvone oxime is a key step in the synthesis of industrially valuable carvone from limonene [2]. Different terpene oximes are widely used as starting compounds and intermediates to obtain important heterocycles, nitriles, amines and carbonyl compounds [3]. Reduction of menthone oxime leads to formation of menthylamine [4] (Figure 1), which is of great practical interest due to its wide application for synthesis of catalysts for chiral phase-transfer [5] and a range of chiral reactions, including hydrosilylation [6, 7, 8], Michael addition [9, 10], asymmetric epoxidation [11, 12] and Henry reactions [13]. Moreover, menthylamine is applied for synthesis of the stationary phase for high performance column chromatography [14]. Based on menthylamine, some biologically active compounds were obtained, including selective antagonists of TRPM8 channels, an important target for neuropathic analgesic drugs [15], as well as antagonists/inverse agonists of cannabinoid CB2 receptors [16].

Menthylamine can be produced from menthone via a multistep reductive amination under Leuckart–Wallach conditions (a thermally driven reaction) or from menthone oxime under Bouveault–Blanc conditions using absolute ethanol and sodium metal and via hydrogenation using a transition metal catalyst [4, 17, 18]. In particular, menthone oxime was reduced using platinum black in glacial acetic acid and Raney nickel in methanol [4, 18]. These approaches resulted in menthylamine formation as a diastereomeric mixture, with the total yield of amine reaching 40-60%. The reaction complexity is related to possible formation of four diastereoisomers, namely, neomenthylamine, menthylamine, isomenthylamine and neoisomenthylamine. In our recent work Pt catalysts based on metal oxides were successfully used for menthone oxime hydrogenation to menthylamine [19]. Menthone oxime hydrogenation over Pt/Al_2O_3 catalysts provided the desired amine formation with the selectivity of 90% at complete oxime conversion. At the same time Pt catalysts application for hydrogenation of oximes, containing several reducible functional groups, such as carvone oxime, led to non-selective hydrogenation of both C=C and C=N bond [19].

As potential catalysts for selective hydrogenation of oximes to amines gold nanoparticles supported on metal oxides can be also considered. Previously it has been demonstrated in our work that Au/TiO_2 catalyst promoted a one-pot synthesis of dihydrocarvone comprising sequential transformations of carvone oxime to dihydrocarvone [20], which is widely used as a flavoring additive in food industry [21]. In that work, application of Au/TiO_2 catalyst for both deoximation and selective hydrogenation of conjugated olefinic C=C functional group was reported for the first time. Note, that unconjugated C=C double bond remained intact. A significant increase in

stereoselectivity towards *trans*-dihydrocarvone was observed when carvone oxime was hydrogenated: the ratio between *trans*- and *cis*-dihydrocarvone was close to 4.0 compared to 1.8 achieved in carvone hydrogenation [2, 22]. However, no amine formation was detected in that work. Generally gold catalysts showed outstanding selectivity and activity in the hydrogen borrowing reactions, as well as in hydrogenation of aldehydes, olefins [23-29]. They are well known as catalysts of the choice for chemoselective hydrogenation of nitro compounds in the presence of reducible functional groups [30-34]. Hydrogenation of nitrocompounds to amines was shown to proceed via an intermediate hydroxylamine derivative formation, while Corma *et al.* obtained oxime from α,β-unsaturated nitrocompounds with H_2 using a gold catalyst [31, 32]. Wang *et al.* reported gas phase hydrogenation of nitrocyclohexane over supported gold catalysts with the oxime being detected among the reaction products [35]. A cooperative effect between the metal and the support to dissociate H_2 and to adsorb the substrate was revealed [33]. It was discussed by Boronat *et al.* that the desired selectivity can be achieved by using a proper support for the nitro group adsorption on the support and at the gold-support interface [33]. Shimizu *et al.* proposed cooperation of the acid-base pair site on alumina and the coordinatively unsaturated Au atoms on Au nanoparticles for heterolytic molecular hydrogen dissociation to H^+/H^- pair at the metal/support interface [32]. Following the latter study utilization of metal oxides containing both acid and basic active sites is preferable.

Generally, utilization of gold catalysts with low hydrogenation activity did often provide higher chemoselectivity compared to conventional hydrogenation over Pt, Pd, Ru catalysts in the case of complicated substrates with several reducible functional group,

such as terpenoids [36, 37]. Herein the research program of the authors on terpene oximes hydrogenation over heterogeneous metal catalysts was further expanded. In the present work the focus was on the gold catalyst design for direct menthone oxime hydrogenation to menthylamine (Figure 1), a compound of a high practical value. To the best of our knowledge, gold catalysts have never been applied for a systematic study of chemoselective oxime hydrogenation. Menthone oxime with a relatively simple structure was selected aiming at further application of the designed catalyst and approaches for more complicated structures of monoterpene oximes, containing reducible functional groups. As expected, Au catalysts can provide higher chemoselectivity compared to conventional Pt catalysts and were successfully applied for selective menthone oxime hydrogenation to menthylamine in the previous work of the authors [19]. On the other hand, it should be noted that menthylamine has three stereocenters resulting in diastereomers formation. A detailed study of mechanistic and kinetics regularities, including dynamics of diastereomers formation, was thus performed with gold containing catalysts.

2. Experimental/methodology

2.1. Preparation of catalysts

Gold catalysts comprising Au (2 wt.%) on metal oxides were prepared by the deposition-precipitation method [38]. Commercial Al_2O_3 (Sasol), ZrO_2 (Alfa-Aesar), TiO_2 (Degussa AG, Aerolyst 7708), and MgO (Vekton) oxides were used as supports. The measured BET surface areas are presented in Table 1. Typically, an aqueous solution of $HAuCl_4$ (1.6×10^{-3} M) and urea (0.21 M) was heated up to 81ºC and the supports in

the powder form (< 63 μm) were added. The slurry was mixed for 4 h at 81ºC and then filtered and washed with water. Additionally, in the case of titania a different concentration of the gold precursor (5×10^{-4} M) and duration of the deposition of 24 h instead of 4 h were applied to vary the gold nanoparticles size. An excess of chloride in the samples after gold deposition was removed by washing with a solution of NH_4OH, as reported in [38, 39]. Thereafter the catalysts were washed thoroughly with deionized water, filtered and dried at room temperature for 24 h. Before the catalytic tests, the samples were pre-treated in air flow increasing temperature to 350ºC with a ramp rate of 2ºC/min.

2.2. Characterization of supports and catalysts

The fresh catalysts were studied by X-ray fluorescence spectroscopy (XRF), nitrogen adsorption technique, transmission electron microscopy (TEM), and X-ray photoelectron spectroscopy (XPS).

The gold content in the synthesized catalysts was analyzed with an XRF with the powder pellet method using an ARL PERFORM'X spectrometer equipped with a rhodium anode X-ray tube (Thermo Fisher Scientific, USA). The porous structure of the catalysts was evaluated by N_2 adsorption in a Micromeritics TriStar II-3020 device (Micromeritics Instrument Corp., USA). Prior the analysis, the samples were degassed in vacuum at 300°C for 4h using a Micromeritics VacPrep 061-Sample degas system (Micromeritics Instrument Corp., USA). The specific surface areas of the catalysts were determined with the Brunauer-Emmett-Teller (BET) method, while the pore size distribution was determined by the BJH model.

The mean size, morphology and elements distribution for supported nanoparticles were determined by STEM using JEM-2010 microscope (JEOL, Japan) with a lattice resolution of 0.14 nm at an accelerating voltage of 200 kV. Prior to analysis, the samples were ultrasonically deposited from a suspension in ethanol on a copper grid coated with a carbon film. The mean diameter was evaluated via measuring more than 150 particles.

The XPS study of the fresh catalysts was performed on photoelectron spectrometer (SPECS Surface Nano Analysis GmbH, Germany) equipped with PHOIBOS-150 hemispherical electron energy analyzer, FOCUS-500 X-ray monochromator, and XR-50M X-ray source with double Al/Ag anode. The core-level spectra were obtained using monochromatic Al Kα radiation ($h\nu$ = 1486.74 eV) and energy of a fixed analyzer pass of 20 eV under ultra-high-vacuum conditions. All measured binding energies were referred to the C1s line of adventitious carbon at 284.8 eV. For detailed analysis, the spectra were fitted into several peaks after background subtraction using the Shirley method. The fitting procedure was performed using CasaXPS software. The line shapes were approximated by the sum of Gaussian and Lorentz functions.

2.3. Catalytic experiments

Methanol (JT Baker) and *L*-menthone (SAFC, *trans*-/*cis*-isomer = 85/15) for the synthesis of menthone oxime were purchased from commercial suppliers and used as received. Menthone oxime was synthesized starting from *L*-menthone according to the method presented in [19]. Menthylamine mixture and (-)-menthone (pure *trans*-isomer)

to study the reaction mechanism were synthesized according to the method presented below.

The catalyst screening was carried out in a batch reactor at 100ºC under H_2 atmosphere (7.5 bar). In a typical experiment, a mixture of menthone oxime (1 mmol), methanol (10 ml) and the catalyst (0.150 g, the active metal to substrate = 1.5 mol %) was intensively stirred. To explore the reaction kinetics, the temperature and hydrogen pressure were varied in the range of 90-110ºC and 5.5-7.5 bar, respectively. The catalytic experiments were performed in the kinetic regime. The internal diffusion limitations were excluded by using the Weisz-Prater criterion [40]. The impact of external diffusion was avoided by conducting experiments at an appropriate stirring speed (1100 rpm).

The catalyst recyclability was studied by scaling the substrate, solvent and the catalyst threefold keeping the ratio between all of them the same. After each reaction run the catalysts was washed with methanol, dried at 100ºC and reused for the next run.

During the reaction the samples of the volume of *ca.* 0.1-0.2 ml were periodically withdrawn and analyzed by gas chromatography: 7820A gas chromatograph (Agilent Tech., USA), HP-5 column (length 30 m, inner diameter 0.25 mm and film thickness 0.25 μm), flame ionization detector operating at 300°C, helium carrier gas (flow rate 2 mL/min, flow division 5:1), temperature range from 120 °C to 280 °C, heating 20 °C/min. Additionally the structure of the products was confirmed by gas chromatography - mass spectrometry (Agilent Tech. 7890 A gas chromatograph with an Agilent 5975C quadrupole mass spectrometer, HP-5MS column, length 30 m, inner diameter 0.25 mm and film thickness 0.25 μm, helium carrier gas, flow rate 1 mL/min, flow division 10:1, temperature range from 50 °C to 280 °C, heating 15 °C/min). ^{1}H- and ^{13}C-NMR spectra

were recorded using a *Bruker DRX-500* spectrometer 500.13 MHz (^{1}H) and 125.76 MHz (^{13}C) in $CDCl_3$ and *Bruker AV-400* spectrometer 400.13 MHz (^{1}H) and 100.61 MHz (^{13}C) in $CDCl_3$. A ratio of stereomeric menthylamines and menthones was determined by high resolution gas chromatography on Agilent 7200 Accurate Mass Q-TOF GC/MS under following conditions: HP-5MS column (length 30 m, inner diameter 0.25 mm and film thickness 0.25 μm); 280 °C GC injector temperature; GC oven temperature range from 50 °C with the temperature holding of 2 min to 280 °C with temperature holding of 5 min, heating 2 °C/min; helium carrier gas (flow division 50:1) with 1 cm^3/min flow rate. The mass spectrometer used electron ionization with 70 eV ionization energy, 230 °C MS ion source temperature, 150 °C MS quadrupole temperature. The signals for amines and ketones were integrated as ions with a maximum contribution in the total ion current (70±0.5 m/z for amines and 112±0.5 m/z for ketones, respectively). The total ion current for each signal was calculated as a maximum intensity of the ion current to maximum intensity ion contribution in the total ion current. The latter was obtained for all diastereomers by analyzing the menthones and methylamines mixtures as a maximum intensity ion current to the total ion current.

TOF values were calculated in two different ways using either moles of converted menthone oxime (Eq. 1) or formed menthylamines (Eq. 2) per mole of exposed catalytic site per unit of time corresponding to the linear part of the kinetic curves according to the following equation:

$$TOF = \frac{n^0 - n}{n_{Me} \cdot D \cdot t} \quad (1)$$

$$TOF^* = \frac{n_{amine}}{n_{Me} \cdot D \cdot t} \quad (2)$$

where n^0 and n are the initial and after 1 h molar amounts of menthone oxime, n_{amine} is molar amounts of menthylamines after 1 h, n_{Me} (mol) the active metal amount in the catalyst, D is the metal dispersion, t is the reaction time, ranging from 0 to 1 h. The metal dispersion was estimated from TEM images for metal nanoparticles using the following equation $D = 8 \cdot r_{Me} / d_{Me}$, where r_{Me} is the metal radius (nm) and d_{Me} is the particle mean diameter (nm). Eq. (1) corresponds to overall transformations of menthone including those involving the acid-base properties of the metal oxide materials, while eq. (2) reflects exclusively hydrogenation on the surface of gold.

2.4 Synthesis of menthylamine (mixture of stereoisomers)

Method 1. Synthesis of menthylamine was performed according to the method described in [41]. Sodium borohydride (2.8 g, 75 mmol) was added to the solution of (*2S*,*5R*)-2-isopropyl-5-methylcyclohexanone oxime (2.1 g, 12 mmol) and $NiCl_2 \cdot 6H_2O$ (5.7g, 24 mmol) in MeOH (40 ml) at -40°C during 4 hours. The resulting mixture was stirred 2 hours at -40°C and then overnight at room temperature. The saturated ammonia solution (20 ml) was added followed by filtering the mixture and extracting with diethyl ether (100 ml). The combined organic layer was washed with brine (20 ml), dried over Na_2SO_4 and evaporated yielding the mixture of menthylamines (65%, 1.3 g, 8.1 mmol). This mixture was analyzed by high resolution gas chromatography. All four diastereoisomers were formed, with neomenthylamine being the main product according to ^{1}H-NMR. The spectrum of the pure neomenthylamine is presented in [42]. Menthylamine and isomenthylamine were assigned using the amines mixture obtained by the method 2 (see below). After the signals of neoisomenthylamine were identified by

excluding signals of other isomers, the ratio of amines was calculated as 60.0:21.0:0.5:18.5 (neomenthylamine : menthylamine : isomenthylamine : neoisomenthylamine).

Method 2. Menthylamine was synthesized following [43]. Sodium (1.1 g, 49 mmol) was added to the solution of (*2S*,*5R*)-2-isopropyl-5-methylcyclohexanone oxime (0.75 g, 4.4 mmol) in absolute ethanol (5.6 ml) under reflux. After the reaction was completed, the mixture was diluted by ethanol (4.7 ml) and treated upon cooling by 2.5M HCl (20 ml) and 10% NaOH (20 ml) solutions consequently, followed by extraction of amines by diethyl ether (3x30 ml). The organic layer was washed with brine (20 ml), dried over Na_2SO_4 and evaporated yielding the mixture of menthylamines (82%, 0.57g, 3.6 mmol). According to [44] only menthylamine and isomenthylamine could be formed. We found by NMR that menthylamine was mainly formed while isomenthylamine and neomenthylamine were minor products. The spectra of the individual isomer are presented in [45].

2.5 Synthesis of (-)-menthone

Synthesis of (-)-menthone was performed according to the method described elsewhere [46]. Commercially available *L*-menthone represents a mixture of *trans*- and *cis*-isomers (85:15). In the current study the trans-isomer was used to explore the reaction scheme. Pyridinium chlorochromate (0.64 g, 3.0 mmol) and silica gel 60 (0.64 g) were ground. The powder was suspended in dichloromethane (6.5 ml) and a solution of (-)-menthol (Sigma-Aldrich, 0.31 g, 2.0 mmol) in dichloromethane (1.5 ml) was added to the resulted mixture. The suspension was stirred at room temperature for 5 hours, eluted with

diethyl ether (20 ml), filtered through silica gel end evaporated yielding (-)-menthone. For removing traces of chromium impurities prior to catalytic experiments a solution of (-)-menthone in hexane (10 ml) was washed by 0.05M EDTA (50 ml), the organic layer was washed with brine (5 ml) dried over Na_2SO_4 and solvent was evaporated. The yield of (-)-menthone was 94% (0.29 g, 1.9 mmol). NMR ^{1}H and ^{13}C are given in Supplementary Materials.

3. Results and discussion

3.1. Catalysts characterization

Specific surface area and porosity of oxides used as supports were determined by nitrogen adsorption. The results are presented in Table 1. Based on XRF the metal loading in the catalysts was in agreement with the theoretical one being *ca.* about 2 wt. Au %.

According to TEM data Au nanoparticles were characterized with an almost semispherical shape practically without well detectable crystallographic planes. Typically, the catalysts were characterized with a uniform and narrow distribution of metal particles. Note, in the case of Au/TiO_2 catalysts synthesized during 24 h some agglomerates with Au nanoparticles size of *ca.* 20 nm were detected by TEM. The agglomerates were found only in a negligible fraction not affecting the monomodal size distribution of gold nanoparticles as well as the average particle size. The latter values are summarized in Table 2, while TEM micrographs are presented in Supplementary Material. In the case of Au/TiO_2 catalysts two type of catalysts were synthesized depending on the preparation technique with average particle sizes of 3.0 and 4.9 nm.

XPS was used to study the chemical state of gold giving the Au4f core-level spectra shown in Figure 2. The Au4f spectra were characterized by the Au $4f_{7/2}$-Au $4f_{5/2}$ doublet, where the peak integral intensities are related as 4:3 and the spin-orbit splitting is 3.67 eV. Only metallic Au species were found for the synthesized catalysts. Depending on the support a slight shift of the $Au4f_{7/2}$ peak was observed. Typically, the binding energy of metallic bulk gold is 84.0 eV. At the same time, Au nanoparticles show a significant shift of the electron binding energy of core levels compared with the bulk values [47]. Moreover, the core level values were demonstrated to depend on the metal oxide support. Particularly, Claus et al. proposed that the binding energy of an electron is influenced by the coordination number of the respective atom, being strongly related to the particle–support interactions [47]. Different position of $Au4f_{7/2}$ peak found in the present work may be related to different character of the particle-support interactions in the tested catalysts. Au nanoparticles supported on titania, alumina, magnesia and zirconia were characterized with the binding energy of $Au4f_{7/2}$ peak at 83.7, 83.8, 83.8 and 83.8 eV, respectively, being in a good agreement with the literature data [38, 48-51]. In the case of gold nanoparticles supported on magnesia the binding energy of $Au4f_{7/2}$ peak was 83.8 eV [52]. Note that for Au/MgO catalyst Au4f spectrum was partly overlapping with the Mg2s spectrum.

3.2. Catalytic results

3.2.1. Catalytic properties of synthesized Au catalysts. Effect of the support nature

In the current study Au catalysts were used for menthone oxime hydrogenation aiming at the development of a catalytic method for menthylamine synthesis and, in general, finding approaches for stereo- and chemoselective hydrogenation of oximes to amines. First, gold nanoparticles supported over different metal oxides such as MgO, Al_2O_3, ZrO_2, TiO_2 were tested in menthone oxime hydrogenation at 100ºC and hydrogen pressure of 7.5 bar using methanol as a solvent to determine an optimal catalyst for a further study of kinetic regularities.

As mentioned above hydrogenation of methone oxime is of interest to produce valuable menthylamine (Fig. 1). While menthylamine has three stereocenters, in the current case only two of them were involved in catalytic processes resulting in four diastereoisomers. The kinetics of the diastereomers formation is discussed below. The second possible direction of the reaction is deoximation to menthone. The route is interesting as an approach for selective deoximation, which in some cases can be of practical interest [20, 53]. The reaction scheme was proposed based on the earlier discussed mechanism of the oximes hydrogenation in the presence of Pd complexes [54]. Note that the intermediate imine seems to be not stable and was not detected in the reaction mixture.

It is worth to note that the metal oxides *per se* were shown to be active in menthone oxime deoximation producing selectively menthone (Table 2). No menthylamine was, however, observed in their presence. Moreover, catalytic activity was noticeably lower compared to the corresponding Au-containing catalysts.

Catalytic behavior was seen to be dependent on the gold nanoparticles size and the support nature (Table 2). Au nanoparticles supported on titania with an average

particle size 4.9 nm promoted menthone oxime deoximation giving *trans*- and *cis*-menthones. The decrease in Au nanoparticles size to 3.0 nm resulted in predominant menthylamine formation. Gold supported on other metal oxides (TiO_2, ZrO_2, Al_2O_3) with the average Au nanoparticle size ranging from 2.0 to 3.0 nm showed similar selectivity to the products and catalyzed hydrogenation of the oxime to the amino group. In the case of gold nanoparticles supported on MgO with a strong basic character selectivity to menthylamine decreased noticeably and deoximation to menthone mainly occurred with selectivity of 53%.

Turnover frequency (TOF) for a series of gold catalysts over different metal oxides depends strongly on the acid-base properties of support (Table 2). A similar trend was observed for TOF* values representing efficiency of the amine formation over Au catalysts (Eq. 2) (Table 2).

Similar to Shimizu et al. [32] analysis of TOF values for gold catalysts along with the electronegativity of the metal ions in metal oxides supports demonstrated that both acidic and basic sites of the support played an important role in menthone oxime hydrogenation to menthylamine. Electronegativity of the metal or a corresponding ion calculated based on the Pauling approach determines the acid–base properties of metal oxides in the way that an increase in electronegativity increases acidity of the metal oxide surface. For applied in this work metal oxides electronegativity of the metals or their ions in support increases in the following order: $MgO<Al_2O_3<ZrO_2<TiO_2$. The highest TOF value among the catalysts with the gold particle size ranging from 2.0 to 3.0 nm was achieved using Au/Al_2O_3. Gold deposited on the support with a basic character such as

MgO and on more acidic metal oxides such as ZrO_2 and TiO_2 showed almost the same catalytic activity.

Thus, small Au nanoparticles (2-3 nm) favored oxime group hydrogenation to amine, whereas the influence of the support nature is also traced. In fact, the former result can be caused by more efficient hydrogen activation over smaller gold nanoparticles [55, 56]. On the other hand, the acid–base properties of the support can affect the dissociative adsorption of hydrogen on the surface of gold catalysts and the substrate adsorption [32]. Detailed discussion on the mechanism scheme based on the obtained results is presented below. Based on the catalysts screening, Au/Al_2O_3 catalyst with the gold nanoparticles size of 2.0 nm as more active and selective in menthone oxime hydrogenation to menthylamine among the tested catalysts was selected for the kinetic study.

3.2.2. Solvent effect

Crucial effect of the solvent nature on the hydrogenation regularities is well known [57]. The solvent can affect the active sites of the catalyst, intermediates/products, reactants *etc.* Particularly, in our previous work the effect of solvent on the catalytic activity and stereoselectivity in carvone hydrogenation to dihydrocarvone was quantitatively described based on the transition state theory and the Kirkwood treatment [22]. The applied theory considered a reaction between ions and dipolar molecules or between two dipolar molecules and the influence of the solvent polarity on the reaction kinetics.

In the current work the effect of the solvent nature on the reaction regularities was explored using apolar and aromatic, polar aprotic and protic solvents, such as hexane,

toluene, tetrahydrofuran (THF), methanol, respectively. Note that the solvent effect was studied using the gold catalyst. The experiments with the gold catalyst and particularly with Au nanoparticles supported on titania with an average particle size 4.9 nm revealed that not only the active sites of the support but also Au species are involved in menthone oxime deoximation. Indeed Au/TiO_2 promoted menthone oxime deoximation giving trans- and cis-menthones with the total yield of 57% compared to 11% over TiO_2 per se after 7 h (Table 2). Since the influence of Au is more important for deoximation than of the support, the impact of the side transformations depending on the solvent was estimated over the gold catalyst, rather than over the support *per se.* Catalytic activity and selectivity to menthylamine were significantly influenced by the solvent in the presence of Au/Al_2O_3 catalyst (Table 2). The highest TOF value was obtained using toluene, with the following reactivity trend toluene > hexane > methanol > THF. At the same time methanol provided noticeably higher selectivity to menthylamine, while other solvents diminished selectivity to the desired amine in a similar manner because of menthone oxime deoximation to menthone. In the latter cases menthones were formed with almost the same selectivity as menthylamines (Table 2). Similarly, toluene utilization in the presence of titania-supported gold catalyst (Au NPs 3 nm) increased the catalytic activity along with the decrease in the selectivity to the amine because of predominant deoximation (Table 2).

In fact, there are numerous parameters that can regulate both the reaction rate and the selectivity to the reaction products. In particular activity can be related to hydrogen solubility, which decreases in the following order: hexane > toluene > THF > methanol [58, 59]. Thus, hydrogen concentration in the solution seems not to limit the reaction.

Another parameter is related to competitive adsorption of the substrates and the solvents on the catalysts surface [57]. However, such influence is crucial when aromatic solvents like toluene, THF are used because of strong adsorption of the solvent on the catalysts surface decreasing the reaction rate. Compared to other solvents applied for menthone oxime hydrogenation methanol has a tendency for dissociative adsorption on the catalysts, forming alkoxides and additional surface hydrogen [57, 60]. Indeed, accumulation of additional hydrogen on the gold-support interface can increase selectivity to the desired amine, being thus significantly higher in methanol. Note that during menthol oxime hydrogenation in methanol traces of the product of the interactions between the methoxide and amine were detected in the reaction mixture. At the same time no transformations of menthone oxime without molecular hydrogen were initiated over the gold catalyst in methanol.

Considering stabilization of the reactants and intermediates by the solvent it was demonstrated that polar solvents provided a lower reaction rate of polar substrates conversion because of stronger interactions between the substrate and the solvent [57]. Particularly the reaction rate of acetophenone hydrogenation was higher in apolar solvents like toluene [61]. In the current study apolar toluene and hexane led to higher activity compared to methanol and THF. A simple analysis considering the transition state theory and the Kirkwood treatment for elementary reactions does not allow correlation of catalytic activity (TOF in Table 2) with the dielectric constant, which increases in the order: hexane < toluene < THF < methanol. Thus, the solvent effect on activity and selectivity in menthone oxime is more complex and cannot be interpreted using a concept of the elementary reactions dependence on solvent polarity. For instance,

already a reaction mechanism comprising two steps [62] is capable of describing optima (maxima or minima as in the current case) for the reaction rates vs. dielectric constant. Moreover, as mentioned above, dissociative adsorption of the solvent can interfere influencing not only activity, but also selectivity. In particular, a noticeably higher selectivity to menthylamine in methanol as a solvent most likely can be attributed to such type of adsorption.

3.2.3. Formal reaction kinetics

To explore the kinetics of menthone oxime hydrogenation the effect of the reaction temperature and hydrogen pressure on the reaction rate and the selectivity to the products was studied in the range 90-110ºC and 5.5-7.5 bar in methanol using Au/Al_2O_3 catalyst. The results are depicted in Figures 3 and 4.

The internal diffusion limitations were excluded by using the Weisz-Prater criterion [40]. For the maximal initial oxime hydrogenation rate ($3 \cdot 10^{-4}$ $mol \cdot l^{-1} \cdot s^{-1}$) the estimated Weisz-Prater modulus was amounted to $\Phi = 0.04$, which indicates absence of any influence of the reaction rate by the substrate diffusion inside the catalyst pores. Due to this criterion no pore limitation occurs, if the Weisz-Prater modulus for the first order reaction is below unity, while for the second order reaction it should be below 0.3. The impact of external diffusion limitations was avoided by conducting experiments at an appropriate stirring speed (1100 rpm).

The hydrogen pressure had no effect on the oxime consumption and overall selectivity to menthylamines within the studied interval (Fig. 3). Thus, the reaction has a zero order with respect to hydrogen pressure. The experimental data for different

temperatures were well described by the equation corresponding to the first order kinetics (Fig. 4a):

$$X = 1 - e^{-k \cdot t}, \quad (2)$$

where X is conversion and k is the rate constant. Plotting ln(k) versus 1/T results in a straight line, as shown in Figure 4b, giving the apparent activation energy calculated from the slope of the Arrhenius plot equal to 46 kJ/mol (with 98% confidence limits). The value of apparent activation energy showed a negligible impact of external diffusion, since otherwise the apparent activation energy is close to 3-10 kJ/mol [40].

As mentioned above, in the current study menthylamine was formed as a mixture of four diastereoisomers, namely neomenthylamine, menthylamine, isomenthylamine, neoisomenthylamine (Fig. 1). To identify the diastereoisomers the synthesis of menthylamine was additionally performed in the current study. Two different approaches were applied giving a mixture of stereoisomers with different composition [41, 43]. The oxime reduction by sodium borohydride in the presence of $NiCl_2$ in methanol resulted in the mixture of diastereoisomers with ratio calculated as 60.0:21.0:0.5:18.5 (neomenthylamine : menthylamine : isomenthylamine : neoisomenthylamine). The reduction of menthone oxime by sodium borohydride in absolute ethanol gave mainly menthylamine while isomenthylamine and neomenthylamine were formed in minor amounts. In the case of menthone oxime hydrogenation over Au/Al_2O_3 predominant formation of neomenthylamine and neoisomenthylamine was detected in the reaction mixture, whereas isomenthylamine was observed in trace amounts. The selectivity to the diastereomers on menthone oxime conversion was independent on both the reaction temperature and the hydrogen pressure (Fig. 5 a, c). During the reaction the

stereoselectivity slightly changed being most likely thermodynamically controlled. Indeed the ratio between diastereoisomers of menthylamine obtained using Au/Al_2O_3 as a catalyst was close to the value for the synthetic method 1 applied in the current study (neomenthylamine (60.0 %), menthylamine (21.0 %), isomenthylamine (0.5 %) and neoisomenthylamine (18.5 %)). Hydrogenation of menthone oxime to the intermediate imine seems to be the rate determining step and further hydrogen addition is controlled by thermodynamics. Based on the literature data in the presence of platinum black in glacial acetic acid the main product was neomenthylamine, while hydrogenation over Raney nickel in methanol led to predominant neoisomenthylamine formation [44]. Thus, utilization of catalysts did not affect the diastereoisomers composition, however, significantly improving efficiency and sustainability of the process. Note that individual diastereomers can be obtained from the resulting mixtures by silica gel column chromatography purification [45] or by crystallization with (+)- and (-)-tartaric acids [63].

Similar to menthylamines the formation of *trans*- and *cis*-menthone was not affected by the reaction temperature and hydrogen pressure (Fig. 5 b, d). The ratio between stereoisomers was close to 4 at almost complete menthone oxime conversion, with thermodynamically more stable *trans*-isomer being obtained predominantly [64, 65]. Note that while the *trans*-isomer of menthone oxime was used as a starting substrate, both *trans*- and *cis*-menthone were detected in the reaction mixture.

An attempt to explore in more detail catalytic isomerization of menthone was performed using neat *trans*-isomer synthesized by (-)-menthol oxidation. First, no thermal isomerization of *trans*-menthone occurred under hydrogen atmosphere. *Trans*-

menthone was reacting very slowly in the presence of the catalyst under the reaction conditions resulting in only 5% *trans*-menthone conversion to *cis*-isomer after 7 h. Addition of menthylamine to *trans*-menthone in a stoichiometric amount resulted in 18% of conversion after 7 h. Utilization of triethylamine instead of menthylamine suppressed isomerization completely. Additionally, no *trans*-menthone isomerization occurred under nitrogen pressure both without the amine and in the presence of menthylamine. Therefore, the results demonstrated a critical feature of menthone isomerization that the primary amine and molecular hydrogen are involved in the transformation.

Thus, a scheme of *trans*- to *cis*-menthone isomerization can tentatively be proposed based on the obtained reaction regularities and a general mechanism of similar transformations. The proposed reaction intermediate formed during isomerization as a result of the initial protonation followed by hydrogen subtraction from the α-carbon via interaction with the amine is presented in Figure 6. Molecular hydrogen, as discussed in details below, underwent heterolytic dissociation on the gold catalyst surface giving hydride ions on gold and protons stabilized on the support, with the latter being initiated menthone isomerization. Such heterolytic dissociation of hydrogen over gold catalysts has been recently discussed in the literature in connection of several heterogeneous catalytic reactions [66, 67].

Menthone isomerization was earlier studied using both homogeneous acidic and basic catalysts including a detailed kinetic study [64, 68, 69]. Bergman observed a larger rate constant for the enolate ion formation from *trans*-menthone compared to the corresponding rate constant for *cis*-menthone, being considered as a rate-limiting step. Generally similar reaction mechanisms were proposed in these studies with some

specificities depending on the catalyst nature. In fact, previously hydrogen was considered as an astoichiometric reactant in *cis-trans* isomerization of substituted cyclohexanols, such as for example 4-tertbutylcyclohexanols [70] or in menthols [71].

Ultimately, to study Au/Al_2O_3 catalyst recyclability, menthone oxime hydrogenation was performed in three consecutive experiments. After each experiment the catalyst was filtered, washed with methanol, dried at 100°C and reused, keeping the same ratio between substrates, the solvent and the catalyst. The catalytic activity increased in each subsequent experiment, whereas selectivity to menthylamine at the same value of menthone oxime conversion (95%) decreased (Fig. 7). Selectivity to menthones and the side products including the product of the interactions between the solvent and amine increased in each subsequent experiment.

The reasons of the catalyst deactivation are most likely related to strong adsorption of the intermediates or the reaction products, which can form oligomeric or polymeric structures. Au/Al_2O_3 catalyst after the third reaction run was characterized by TEM (Fig. 8a). Compared to the fresh sample the gold particles size increased just slightly while the carbon deposits, which may block the active sites, were clearly detected on the surface. Leaching of the active phase, as another reason for catalyst deactivation, was excluded based on the XRF analysis. In our previous work a drastic reduction of the catalytic activity was observed during one-pot myrtenol amination with aniline over Au/ZrO_2 catalyst because of the intermediate imine oligomerization or polymerization and subsequent blocking of the active sites [72]. At the same time, in the case of menthone oxime hydrogenation, its conversion was not influenced giving just a gradual decrease in selectivity to menthylamine. Thus, deactivation mainly affected the active

sites required for hydrogenation to the amine. An attempt to restore selectivity to menthylamine by Au/Al_2O_3 catalyst regeneration was performed. The catalyst after the third reaction run was subjected to the treatment in an air flow up to 450ºC with the heating rate 10º/min. According to TEM data the gold particle size in Au/Al_2O_3 did not change after the treatment (Fig. 8b). At the same time catalyst regeneration did not completely restore the catalytic activity and almost the same catalytic activity and selectivity to desired menthylamine were achieved as for the third reaction run (Fig. 7).

3.2.4. Discussion on the reaction mechanism

In our recent study on monoterpenoid oximes hydrogenation over platinum catalysts possible reaction scheme was discussed [19]. It was proposed that the oxime hydrogenation proceeds via imine formation followed by its further hydrogenation or hydrolysis depending on the nature of the catalyst [19, 54]. Similar to Pt catalysts, no transformations of menthone oxime to both menthones and menthylamines were observed without molecular hydrogen over the gold nanoparticles on metal oxides. At the same time menthylamine was obtained over the gold nanoparticles with a proper particle size close to 2-3 nm.

Earlier Corma *et al.* observed oxime formation during hydrogenation of α,β-unsaturated nitrocompounds by molecular hydrogen using a gold catalyst that tentatively showed some common features in the substrate activation on the catalyst surface for the reduction of nitrocompounds and oximes [31]. Based on DFT calculations, it was proposed that chemoselective hydrogenation of a nitro group in nitrostyrene over Au/TiO_2 proceeded via H_2 dissociation, while energetically and geometrically favored

adsorption through the nitro group occurred on titania and in the interface between the low coordinated gold nanoparticle and the support [33]. In addition, Shimizu *et al.* demonstrated for a highly active Au/Al_2O_3 catalyst using FTIR *in-situ* that nitrostyrene interacts with alumina through the nitro group. Molecular hydrogen underwent heterolytic dissociation on the surface of Au/Al_2O_3 giving hydride ions on low coordinated Au atoms and protons stabilized at the oxygen atoms of the support [32, 73].

Based on the data obtained in the current study and the literature data the reaction scheme can be proposed for gold catalysts (Fig. 9). In the case of menthone oxime hydrogenation independent on the reaction route the substrate is adsorbed on the metal oxide (MeO, Fig. 9) surface interacting with it through the oxime group. Subsequently for both routes activation most likely proceeds via a proton transfer from the support surface. The presence of gold nanoparticles increased the initial reaction rate because of heterolytic hydrogen dissociation generating available hydrogen species [73]. Such dissociation leads to formation of Au_n-$H^{\delta-}$ and $MeOH^{\delta+}$ (Fig. 9). It is worth to emphasize that it was experimentally and theoretically demonstrated that low coordinated gold atoms were required for dissociative adsorption of H_2 and the average number of dissociatively adsorbed hydrogen atoms increased with decreasing the particle size being limited to the gold atoms on corner and edge positions [55, 56]. Thus, smaller gold nanoparticles provided more efficient hydrogen activation favoring oxime hydrogenation to the amino group via a transfer of H^+/H^- species from the metal-support interface to the polar bond (Fig. 9). Alternatively, a lack of active hydrogen species on the catalyst surface as well as metal oxides with a basic character resulted in a transfer of hydroxyl species from the support giving menthone (Fig. 9). Note that the presence of hydroxyl

species on the support surface can be related also to dissociative methanol adsorption [74]. In fact, an increase in selectivity to menthone over gold supported on basic magnesia is in line with this hypothesis.

Therefore, gold nanoparticles seem to act in tandem with the metal oxide during menthone oxime transformation. Both menthone oxime and molecular hydrogen activation proceeded by involving active sites of the support, with the acid-base properties of the support being important. Gold nanoparticles with a proper size (2-3 nm) provided more efficient hydrogen activation.

4. Conclusions

In the current study gold nanoparticles supported over different metal oxides such as magnesia, titania, zirconia and alumina were utilized for menthone oxime hydrogenation. For the first time gold catalysts were shown to be efficient for the synthesis of valuable menthylamine. Gold nanoparticles and metal oxides used as a support seem to act in tandem. The initial adsorption of menthone oxime was proposed to proceed on the support surface, while molecular hydrogen is dissociated giving a hydride ion on the low coordinated Au atom and proton stabilized at the oxygen atom of the support. An increase of gold nanoparticles size and utilization of metal oxides with a strong basic character such as magnesia favored deoximation to menthone. A higher catalytic activity and selectivity to menthylamine was achieved in the presence of Au/Al_2O_3 catalyst. Gold supported on more acidic metal oxides such as ZrO_2 and TiO_2 showed a lower catalytic activity compared to alumina displaying similar selectivity to menthylamine. Kinetics of menthone oxime hydrogenation was studied over Au/Al_2O_3 catalyst. The catalytic activity and the selectivity to menthylamine were noticeably influenced by the solvent nature, with higher selectivity to the amine achieved using methanol. The reaction has zero and first orders with respect to hydrogen pressure and menthone oxime concentration, respectively. Stereoselectivity to menthylamines and menthones was independent on the reaction temperature and the hydrogen pressure, being more affected by thermodynamics. Au/Al_2O_3 catalyst recyclability was studied in three consecutive experiments. A gradual decrease of selectivity to menthylamine was observed, whereas the catalytic activity did not suffer. The deactivation mainly affected

the active sites required for hydrogenation to the amine most likely related to strong adsorption of the intermediates or reaction products, which can form oligomeric or polymeric structures.

Acknowledgements

The authors acknowledge the Multi-Access Chemical Research Center SB RAS and the Center of Collective Use «National Center of Catalyst Research» of Boreskov Institute of Catalysis for spectral and analytical measurements. This work was supported by the Russian Foundation for Basic Research grant № 18-33-20175 and by Ministry of Science and Higher Education of the Russian Federation project no. AAAA-A17-117041710075-0.

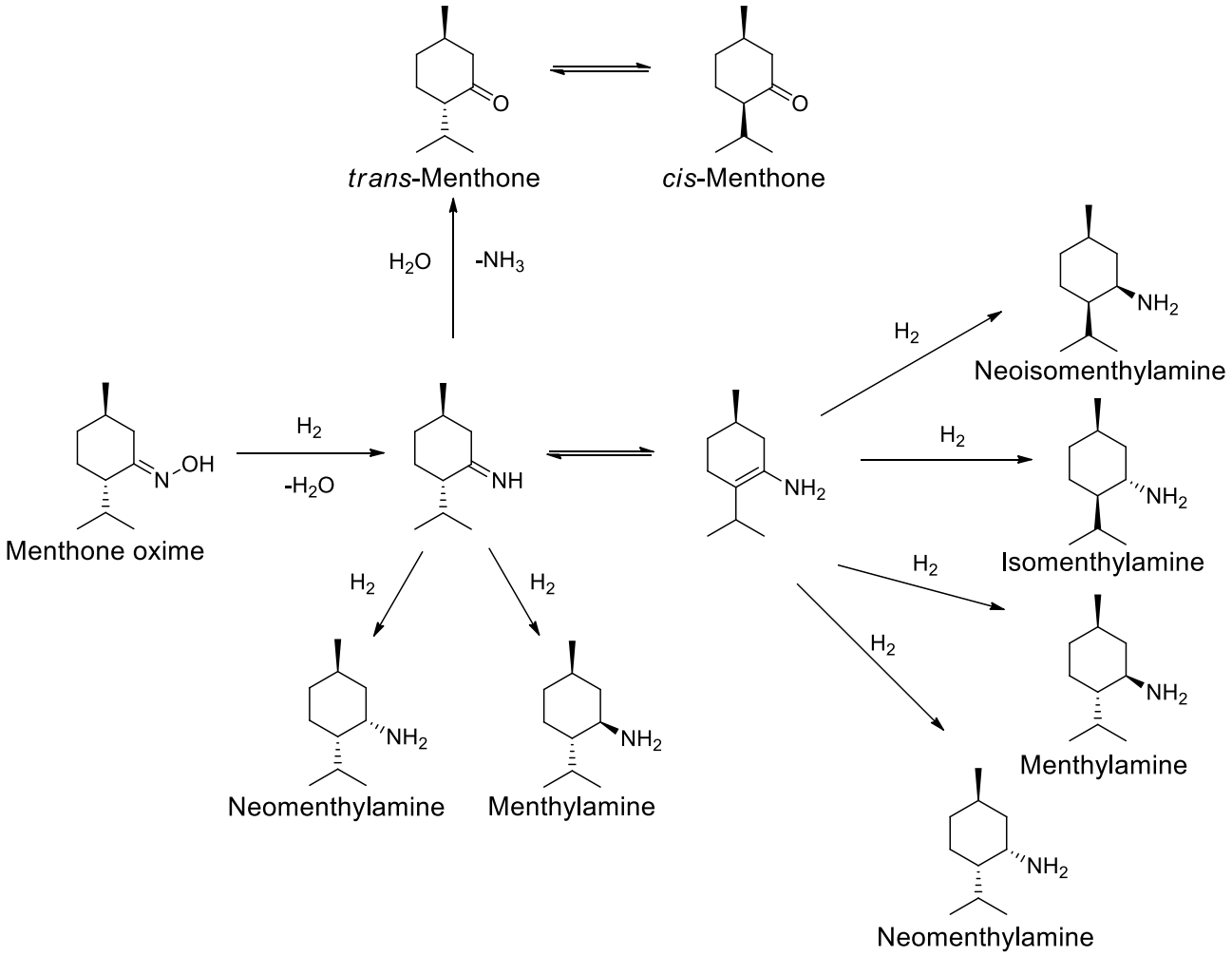

Figure 1. Scheme of gold-catalyzed transformation of menthone oxime under hydrogen atmosphere.

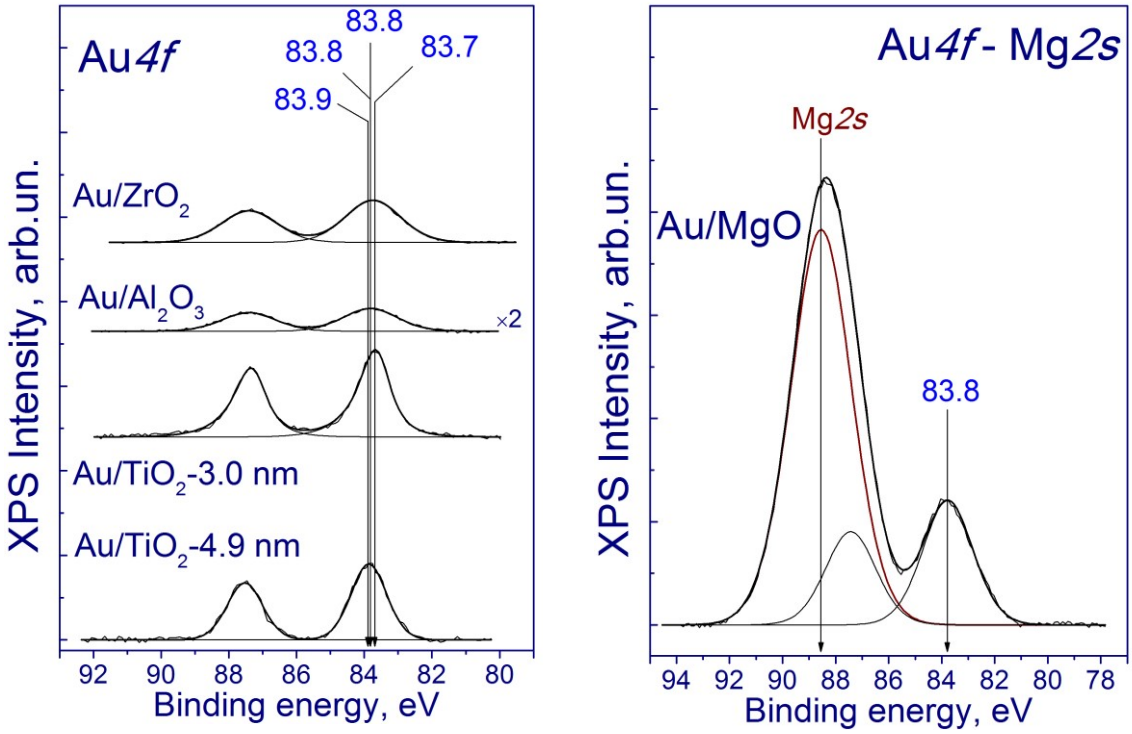

Figure 2. XPS spectra of Au catalysts (symbols – experimental data, curves – fitting).

Table 1. Specific surface area and pores of oxides used as supports.

Sample	S_{BET}, m^2/g	Pore volume, cm^3/g	Pore diameter, nm
MgO	33	0.2	22.6
Al_2O_3	204	0.5	10.3
ZrO_2	103	0.3	10.8
TiO_2	45	0.2	7.6

Table 2. Average particle sizes according to TEM measurements and catalytic properties of gold catalysts after 7 h. The reaction conditions: T = 100°C, p (H_2) = 7.5 bar, menthone oxime 1 mmol, solvent 10 ml, catalyst 150 mg (Me/menthone oxime = 1.5 mol.%).

Sample	NPs size, nm	Solvent	TOF[d], h^{-1}	TOF*[e], h^{-1}	Conversion, %	Selectivity, %	
						Menthylamines[f]	Menthones[f]
TiO_2	-	methanol	-	-	14	0	82
ZrO_2		methanol		-	20	0	100
Al_2O_3	-	methanol	-	-	38	0	92
MgO		methanol		-	22	0	91
Au/TiO_2[a]	4.9	methanol	54	5.6	82	10	70
Au/TiO_2	3.0	methanol	21	14.2	73	62	13
Au/TiO_2[c]		methanol	21	14.2	80	61	13
Au/TiO_2		toluene	32	9.2	99	29	66
Au/ZrO_2	2.1	methanol	18	12.3	79	67	13
Au/ZrO_2[c]		methanol	18	12.3	85	66	13
Au/Al_2O_3	2.0	methanol	30	20.1	99	64	18
Au/Al_2O_3		toluene	45	19.3	98	43	41
Au/Al_2O_3		hexane	34	16.5	97	48	37
Au/Al_2O_3		THF	19	8.3	65	45	48
Au/MgO	3.0	methanol	20	4.7	63	24	53
Au/MgO[c]		methanol	20	4.7	76	26	57

[a]Au/TiO_2 catalyst was synthesized using an aqueous solution of $HAuCl_4$ with the concentration of 5×10^{-4} M during 24 h;

[b]The reaction was performed using toluene as a solvent;

[c]Conversion after 9 h;

[d]Total turnover frequency was calculated after 1 h according to Eq. 1;

[e]Total turnover frequency was calculated after 1 h according to Eq. 2;

[f]Overall selectivity to menthylamine and menthone, respectively.

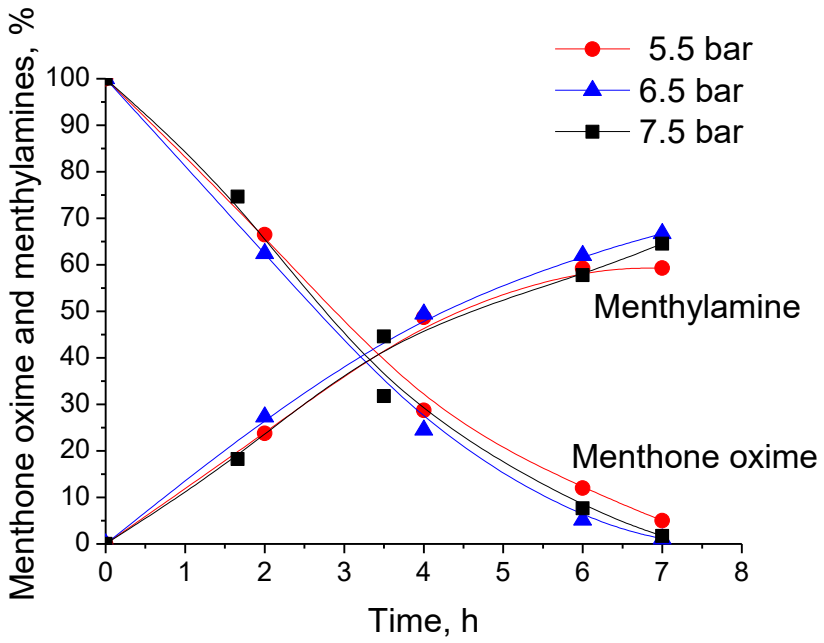

Figure 3. Effect of hydrogen pressure on menthone oxime consumption and menthylamines formation over Au/Al_2O_3 catalyst. The reaction conditions: T = 100°C, p (H_2) = 5.5-7.5 bar, menthone oxime 1 mmol, methanol 10 ml, catalyst 150 mg (Me/menthone oxime = 1.5 mol.%).

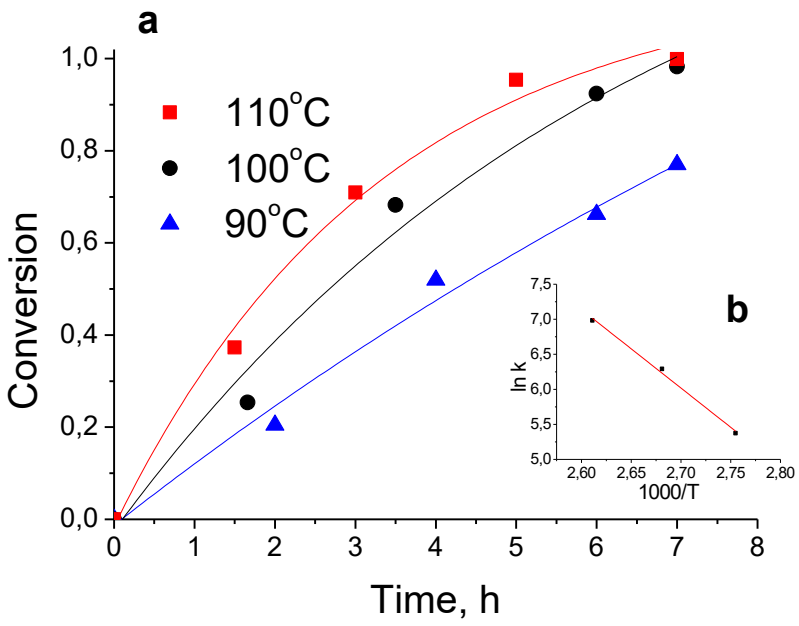

Figure 4. Menthone oxime conversion vs. reaction time at different temperature over Au/Al_2O_3 catalyst (a) and Arrhenius plot of rate constant of menthone oxime hydeogenation (b). The reaction conditions: T = 90-110°C, p (H_2) = 7.5 bar, menthone oxime 1 mmol, methanol 10 ml, catalyst 150 mg (Me/menthone oxime = 1.5 mol.%).

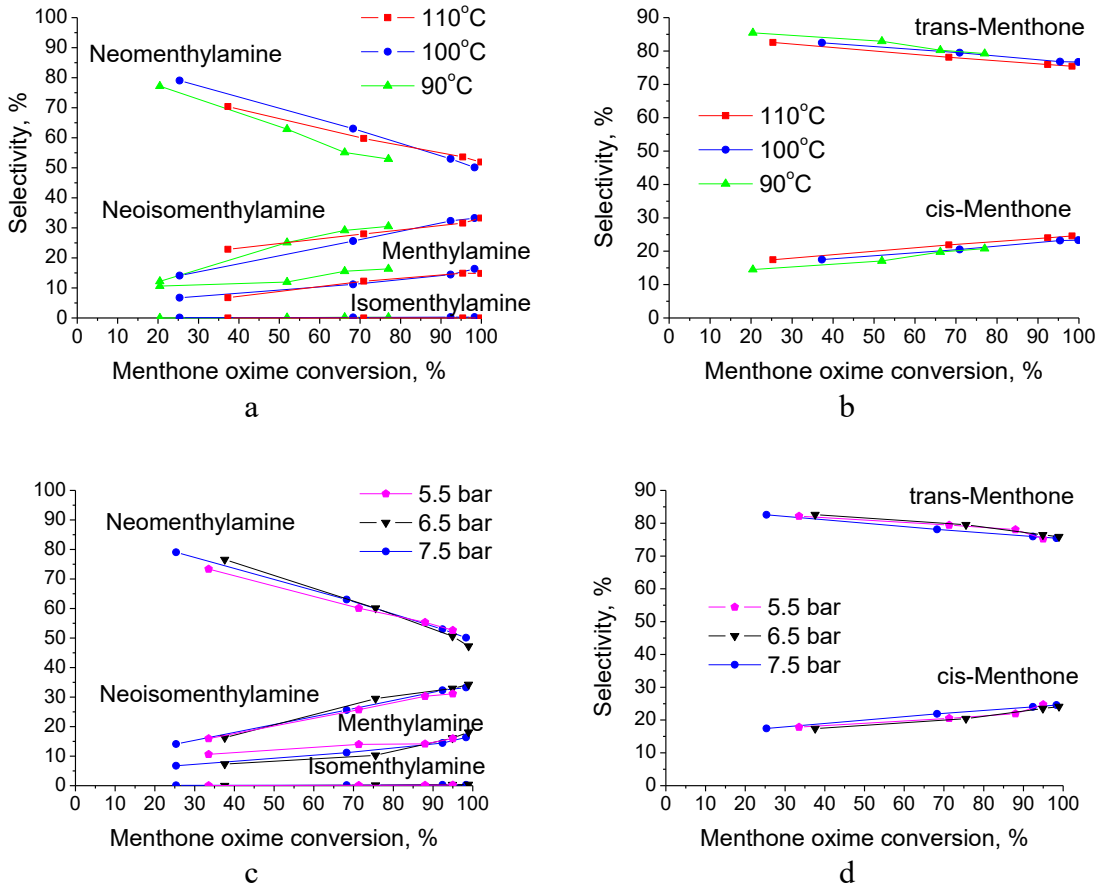

Figure 5. Selectivity to menthylamines (a, c) and menthones (b, d) vs. reaction time at different reaction temperature and hydrogen pressure. The reaction conditions: T = 90-110°C, p (H_2) = 5.5-7.5 bar, menthone oxime 1 mmol, methanol 10 ml, Au/Al_2O_3 catalyst 150 mg (Me/menthone oxime = 1.5 mol.%).

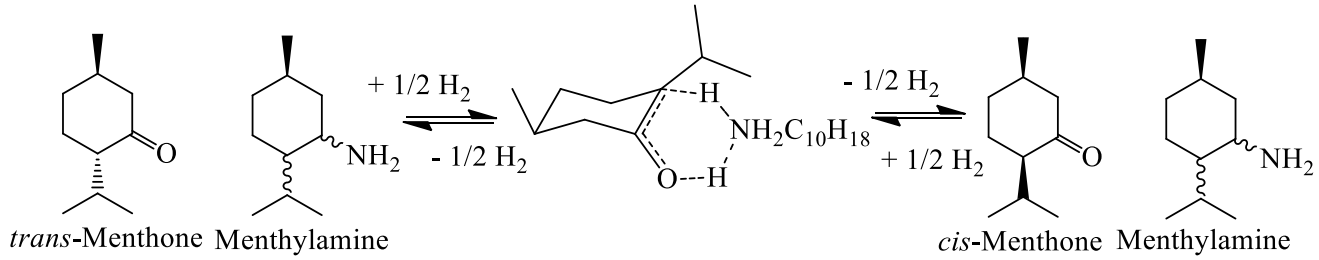

Figure 6. The intermediate of catalytic *trans*- to *cis*-menthone isomerization in the presence of menthylamine.

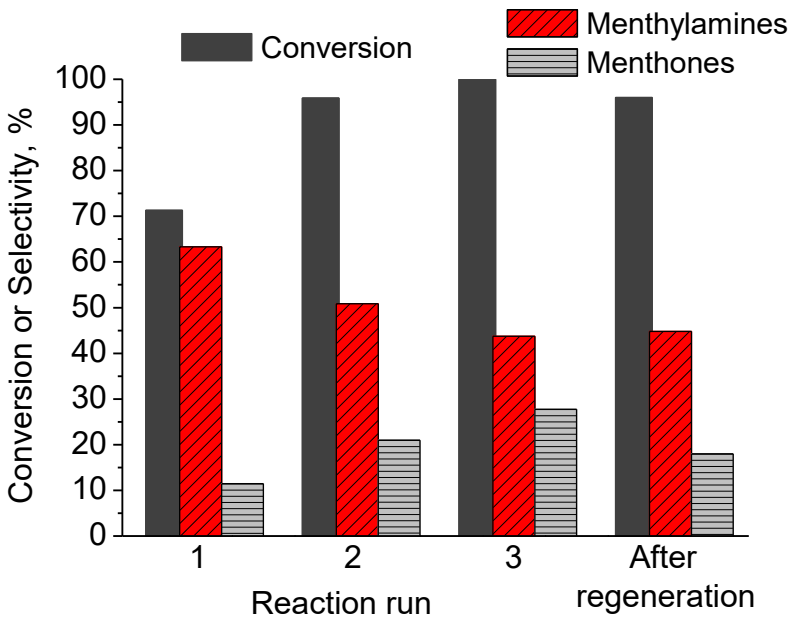

Figure 7. Menthone oxime conversion after 4 h and selectivity to the main products at the same menthone oxime conversion (95%) at 100°C and hydrogen pressure of 7.5 bar for Au/Al_2O_3 recycling and regeneration in air flow up to 450°C (10º/min).

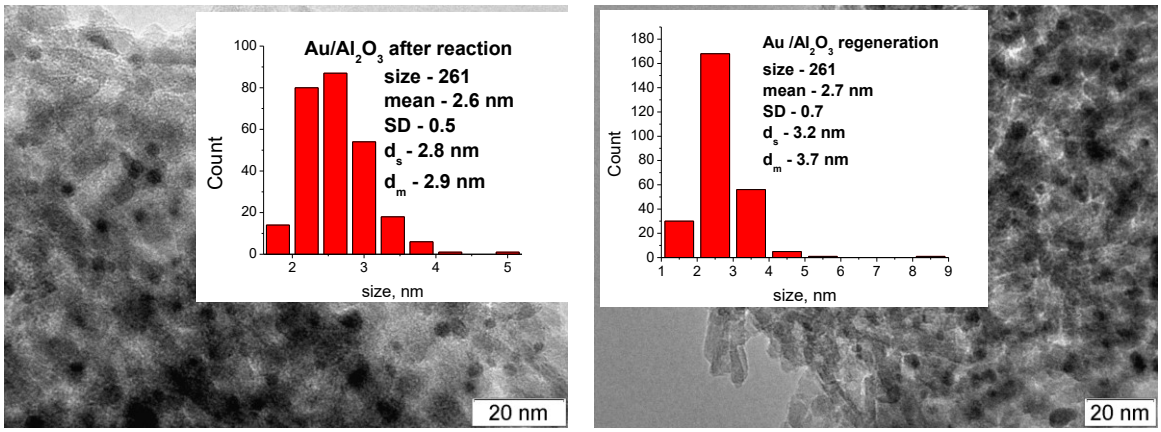

a b

Figure 8. TEM micrographs and histograms of Au/Al_2O_3 catalyst: (a) after third reaction run and (b) the catalyst regeneration in air flow up to 450°C (10º/min). The reaction conditions: T = 100°C, p (H_2) = 7.5 bar, menthone oxime 1 mmol, methanol 10 ml, catalyst 150 mg (Me/menthone oxime = 1.5 mol.%).

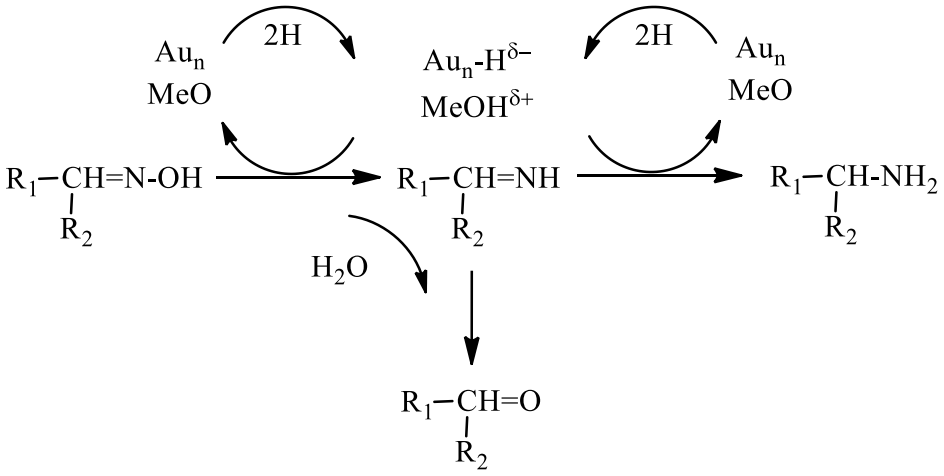

Figure 9. A mechanistic scheme of gold-catalyzed menthone oxime hydrogenation (MeO – metal oxide support).

References

[1] N.F. Salakhutdinov, K.P. Volcho, O.I. Yarovaya, Pure Appl. Chem. 89 (8) (2017) 1105-1118.

[2] E. Lück, G. von R. Lipinski, Foods, 3. Food Additives, Ulmann's Encycl. Ind. Chemostry. (2012) 671–692.

[3] Z. Rappoport, J.F. Liebman, The Chemistry of Hydroxylamines, Oximes and Hydroxamic Acids, John Wiley & Sons, Ltd 2009.

[4] N.G. Kozlov, Chem. Nat. Compd. 18 (1982) 131–143.

[5] S. Kumar, M.E. Sobhia, U. Ramachandran, Tetrahedron Asymmetry. 16 (2005) 2599–2605.

[6] M. Steinbeck, G.D. Frey, W.W. Schoeller, W.A. Herrmann, J. Organomet. Chem. 696 (2011) 3945–3954.

[7] V.M. Uvarov, D.A. de Vekki, V.P. Reshetilovskii, N.K. Skvortsov, Russ. J. Gen. Chem. 80 (2010) 35–46.

[8] D.A. de Vekki, V.M. Uvarov, A.N. Reznikov, N.K. Skvortsov, Russ. Chem. Bull. 57 (2008) 349–357.

[9] D. Ma, K. Cheng, Tetrahedron Asymmetry. 10 (1999) 713–719.

[10] Y. Zhou, Q. Liu, Y. Gong, Org. Biomol. Chem. 10 (2012) 7618–7627.

[11] P.C. Bulman Page, G.A. Rassias, D. Barros, D. Bethell, M.B. Schilling, J. Chem. Soc. Perkin Trans. 1. 2 (2000) 3325–3334.

[12] P.C.B. Page, G.A. Rassias, D. Bethell, M.B. Schilling, A J. Org. Chem. 63 (1998) 2774–2777.

[13] Y. Zhou, Y. Gong, Asymmetric European J. Org. Chem. (2011) 6092–6099.

[14] Bömer, B.; Großer, R.; Lange, W.; Zweering, U.; Köhler, B.; Sirges, W.; Grose-Bley, M. DE19546136A1, 1997; Chem. Abstr. 1997, 127, 96037.

[15] G. Ortar, L. De Petrocellis, L. Morera, A.S. Moriello, P. Orlando, E. Morera, M. Nalli, V. Di Marzo, Bioorganic Med. Chem. Lett. 20 (2010) 2729–2732.

[16] A. Dore, B. Asproni, A. Scampuddu, S. Gessi, G. Murineddu, E. Cichero, P. Fossa, S. Merighi, S. Bencivenni, G.A. Pinna, Bioorganic Med. Chem. 24 (2016) 5291–5301.

[17] C. Edinger, J. Kulisch, S.R. Waldvogel, Beilstein. J. Org. Chem. 11 (2015) 294-301.

[18] H. Feltkamp, F. Koch, T. N. Thanh, Justus Liebigs Ann. Chem. 707 (1967) 78–86.

[19] Yu.S. Demidova, E.S. Mozhaitsev, A.A. Munkuev, E.V. Suslov, A.A. Saraev, K.P. Volcho, N.F. Salakhutdinov, I.L. Simakova, D.Yu. Murzin, Top. Catal. 63 (2020) 187-195.

[20] Yu.S. Demidova, E.V. Suslov, O.A. Simakova, I.L. Simakova, K.P. Volcho, N.F. Salakhutdinov, D.Yu. Murzin, J. Mol. Catal. 420 (2016) 142-148.

[21] K.-G. Fahlbusch, F.-J. Hammerschmidt, J. Panten, W. Pickenhagen, D. Schatkowski, K. Bauer, H. Surburg. Flavors and fragrances. In Ullmann's Encyclopedia of Industrial Chemistry. Vol 15, 73-198, Wiley-VCH Verlag GmbH & Co. KGaA, 2003.

[22] Yu.S. Demidova, E.V. Suslov, O.A. Simakova, I.L. Simakova, K.P. Volcho, N.F. Salakhutdinov, D.Yu. Murzin, Catal. Today 241 (2015) 189-194.

[23] P. Claus, Appl. Catal. A: Gen. 291 (2005) 222-229.

[24] Yu.S. Demidova, I.L. Simakova, M. Estrada, S. Beloshapkin, E.V. Suslov, D.V. Korchagina, K.P. Volcho, N.F. Salakhutdinov, A.V. Simakov, D.Yu. Murzin, Appl. Catal.A: Gen. 464–465 (2013) 348–356.

[25] Yu. S Solkina, S. Reshetnikov, M. Estrada, A.V. Simakov, D.Yu. Murzin, I.L. Simakova. Chem. Eng. J. 176-177 (2011) 42-48.

[26] C. Milone, R. Ingoglia, A. Pistone, G. Neri, F. Frusteri, S. Galvano, J. Catal. 222 (2004) 348-356.

[27] C. Milone, R. Ingoglia, L. Schipilliti, C. Crisafulli, G. Neri, S. Galvano, J. Catal. 236 (2005) 80-90.

[28] C. Milone, C. Crisafulli, R. Ingoglia, L. Schipilliti, S. Galvano, Catal. Today 122 (2007) 341-351.

[29] A. S. K. Hashmi, G. J. Hutchings, Angew. Chem. 45 (2006) 7896-7936.

[30] A. Corma, P. Serna, Science, 313 (2006) 332-334.

[31] A. Corma, P. Serna,H. Garcia, J. Am. Chem. Soc. 129 (2007) 6358-6359.

[32] K. Shimizu, Y. Miyamoto, T. Kawasaki, T. Tanji, Y. Tai, A. Satsuma, J. Phys. Chem. 113 (2009) 17803-17810.

[33] M. Boronat, P. Concepciòn, A. Corma, S. Gonzàlez, F. Illas, P. Serna, J. Am. Chem. Soc. 129 (2007) 16230-16237.

[34] P. Serna, M. Boronat, A. Corma, Top. Catal. 54 (2011) 439-446.

[35] X. Wang, N. Perret, M. A. Keane, Appl. Catal. A: Gen. 467 (2013) 575-584.
[36] J.A. Becerra, Ó.F. Arbeláez, A.L. Villa, Brazilian J. Chem. Eng. 37 (2020) 1–27.
[37] M. Sankar, Q. He, R.V. Engel, M.A. Sainna, A.J. Logsdail, A. Roldan, D.J. Willock, N. Agarwal, C.J. Kiely, G.J. Hutchings, Chem. Rev. 120, 8 (2020) 3890-3938.
[38] E. Smolentseva, B.T. Kusema, S. Beloshapkin, M. Estrada, E. Vargas, D.Y. Murzin, F. Castillon, S. Fuentes, A. Simakov, Appl. Catal. A: Gen. 392 (2011) 69-79.
[39] S. Ivanova, V. Pitchon, Y. Zimmermann, C. Petit, Appl. Catal. A 298 (2006) 57-64.
[40] D. Murzin, T. Salmi, Catalytic Kinetics, Elsevier, Amsterdam, 2005, pp. 341-418.
[41] Y. Zhou, J. Dong, F. Zhang, Y. Gong, J. Org. Chem. 76 (2) (2011) 588-600.
[42] T. C. Pickel, G. J. Karahalis, C. T. Buru, J. Bacsa, C. C. Scarborough. Eur. J. Org. Chem. 2018 (48) (2018) 6876-6889.
[43] H. Feltkamp, F. Koch, T. N. Thanh, Justus Liebigs Ann. Chem. 707 (1967) 78-86.
[44] N. G. Kozlov. Chem. Nat. Compd. 18 (2) (1983) 131–143.
[45] J. Kulisch, M. Nieger, F. Stecker, A. Fischer, S. R. Waldvogel, Angew. Chem. 50 (24) (2011) 5564-5567.
[46] Y. Murakami, Y. Takeda, S. Minakata. J. Org. Chem. 76 (15) (2011) 6277-6285.
[47] J. Radnik, C. Mohr, P. Claus, Phys. Chem. Chem. Phys. 5 (2003) 172-177.
[48] F.-W. Chang, H.-Y. Yu, L.S. Roselin, H.-C. Yang, T.-C. Ou, Appl. Catal. A 302 (2006) 157–167.
[49] P. Konova, A. Naydenov, C. Venkov, D. Mehandjiev,D. Andreeva, T. Tabakova, J. Mol. Catal. 213 (2004) 235–240.
[50] I.L. Simakova, Yu. S. Demidova, M. Estrada, S. Beloshapkin, E.V. Suslov,K.P. Volcho, N.F. Salakhutdinov, D.Yu. Murzin, A. Simakov, Catal. Tod. 279 (2017) 63–70.
[51] Yu.S. Demidova, I.L. Simakova, M. Estrada, S. Beloshapkin, E.V. Suslov, D.V. Korchagina, K.P. Volcho, N.F. Salakhutdinov, A.V. Simakov, D.Yu. Murzin, Appl. Catal. A 464– 465 (2013) 348– 356.
[52] X. Cao, J. Zhou, H. Wang, S. Li, W. Wang, G. Qin, J. Mater. Chem. A 7 (2019) 10980-10987.

[53] K.-G. Fahlbusch, F.-J. Hammerschmidt, J. Panten, W. Pickenhagen, D. Schatkowski, K. Bauer, H. Surburg. Flavors and fragrances. In Ullmann's Encyclopedia of Industrial Chemistry. Vol 15, 73-198, Wiley-VCH Verlag GmbH & Co. KGaA, 2003.
[54] Y. Liu, Z. Quan, S. He, Z. Zhao, J. Wang, B. Wang, React. Chem. Eng. 4 (2019) 1145-1152.
[55] A. Corma, M. Boronat, S. Gonzàlez, F. Illas, Chem. Commun. 32 (2007) 2007, 3371-3373.
[56] E. Bus, J. T. Miller, J. A. van Bokhoven, J. Phys. Chem. B, 109 (2005) 14581-14587.
[57] J.J. Varghese, S.H. Mushrif, React. Chem. Eng. 4 (2019) 165-206.
[58] E. Brunner, J.Chem Eng. Data 30 (3) (1985) 269-273.
[59] Hydrogen and deuterium. Solubility data series. Volume 5/6, Pergamon Press, Oxford, 1981, 646 pp.
[60] Yu.S. Demidova, E.V. Suslov, I.L. Simakova, K.P. Volcho, E. Smolentseva, N.F. Salakhutdinov, A.V. Simakov, D.Yu. Murzin, Mol. Catal. 433 (2017) 414-419.
[61] N. M. Bertero, A. F. Trasarti, C. R. Apesteguía and A. J. Marchi, Appl. Catal., A, 2011, 394, 228–238.
[62] D.Yu. Murzin, Catal. Sci. Technol. 6 (2016) 5700-5713.
[63] N. Welschoffa, S. R. Waldvogel, Synthesis 21 (2010) 3596-3601.
[64] N. Bergman, Acta Chem. Scand. A 33 (1979) 577-582.
[65] B. Rickborn, J. Am. Chem. Soc. 84 (1962) 2414-2417.
[66] T. Whittaker, K. B. Sravan Kumar, C. Peterson, M.N. Pollock, L.C. Grabow, B.D. Chandler, J. Am. Chem. Soc. 140 (48) (2018) 16469-16487.
[67] R. Juárez, S.F. Parker, P. Concepción, A. Corma, H. García, Chem. Sci., 1 (2010) 731-738.
[68] J.F. Bunnett, L.A. Retallick, J. Am. Chem. Soc. 89 (1967) 423-428.
[69] Y. Pocker, R.F. Buchholz, J. Am. Chem. Soc. 93 (1971) 2905-2909.
[70] D.Yu. Murzin, Kinet. Catal. 34 (1993) 495-499.
[71] B. Etzold, A. Jess, M. Nobis, Catal. Today 140 (1-2) (2009) 30–36.
[72] Yu.S. Demidova, I.L. Simakova, J. Wärnå, A.V. Simakov, D.Yu. Murzin, Chem. Eng. J. 238 (2014) 164-171.

[73] E. Bus, J.T. Miller, J.A. van Bokhoven, Phys. Chem. B 109 (30) (2005) 14581-14587.
[74] M.M. Branda, R.M. Ferullo, P.G. Belelli, N.J. Castellani, Surf. Sci. 527 (2003) 89-99.